
Zero-Error Tracking for Autonomous Vehicles through Epsilon-Trajectory Generation

Clint Ferrin · Greg Droge · Randall Christensen

Abstract This paper presents a control method and trajectory planner for vehicles with first-order nonholonomic constraints that guarantee asymptotic convergence to a time-indexed trajectory. To overcome the nonholonomic constraint, a fixed point in front of the vehicle can be controlled to track a desired trajectory, albeit with a steady-state error. To eliminate steady state error, a sufficiently smooth trajectory is reformulated for the new reference point such that, when tracking the new trajectory, the vehicle asymptotically converges to the original trajectory. The resulting zero-error tracking law is demonstrated through a novel framework for creating time-indexed Clothoids. The Clothoids can be planned to pass through arbitrary waypoints using traditional methods yet result in trajectories that can be followed with zero steady-state error. The results of the control method and planner are illustrated in simulation wherein zero-error tracking is demonstrated.

Keywords nonholonomic systems, motion planning, feedback control, autonomous vehicles, mobile robots, dynamic partial feedback linearization.

1 Introduction

The control of mobile robots continues to be a focus of academic and industrial research, especially due to a demand for high-precision path following for a variety of mobile robots. Though the dynamic equations for mobile robots can vary dramatically, they share similar trajectory-tracking limitations due to their nonholonomic constraints and nonlinear equations of motion that warrant continued research for vehicle control and path planning e.g. [9].

One limitation of vehicles with first-order nonholonomic constraints is that they cannot move orthogonal to their direction of motion [14]. This limitation is overcome through various approaches including open-loop control [16], linearizing about a trajectory [5], or reformulating the control problem using a path-

C. Ferrin
Utah State University, Logan, Utah 84322 USA
Tel.: +1-435-554-8176
E-mail: clint.ferrin@gmail.com

following controller that is not time-dependent [1]. The most common approach is to use a path-following controller which separates the system into two separate controllers [1, 9]. One controller governs the vehicle's velocity, while the other controller uses the vehicle's steering input to converge to the desired path. Though the path-following controller addresses the issue of controllability, new complexities arise such as how to treat self-intersecting paths, and how to optimally calculate which point on the path to use as a reference because the problem is not time-dependent.

An alternative approach is to control a point on the robot that does not have a nonholonomic constraint. Instead of controlling the center point of a fixed axle, [17] showed that a point ϵ in front could be controlled as if it were unconstrained, allowing for partial feedback linearization. The inputs of the unconstrained control can then be mapped algebraically to the control inputs of the vehicle, and the reference trajectory is tracked with a steady-state error of ϵ . This control technique is referred to as ϵ -tracking, and the theoretical limit for ϵ is solely that it remains positive, allowing the reference tracking error to become arbitrary small [17]. In practice, however, very small values of ϵ can become problematic due to noise introduced by dynamics, sensors, or even numeric integration. Therefore, the first major contribution of this paper is to generate a new trajectory that, when followed using ϵ -tracking, results in zero-error, asymptotic tracking of the vehicle control point to the original reference trajectory. The new tracking law is referred to as zero-error ϵ -trajectory tracking.

Another common limitation for mobile vehicles that must be taken into account when developing trajectories for vehicles is the executability of a trajectory. The maximum curvature limitation for path planning is commonly addressed with the Dubins path, which is formed using a waypoint path planner that produces optimal distance paths between two oriented points using circular arcs and straight lines while taking into account maximum curvature constraints [6]. Dubins paths, however, require instantaneous changes in curvature which is often not achievable in physical systems due to actuator limitations and wheel slippage [15]. Fraichard and Scheuer proposed adapting the Dubins path by connecting waypoints using straight lines, circular arcs, and transition arcs to account for the maximum change of curvature [7], which are referred to as continuous curvature paths (CCPaths). The addition of the transition arc maintains curvature continuity between circles and lines. The second contribution of this research is to convert CCPaths paths into trajectories with corresponding feed-forward terms which can be used for control. The result of these contribution is a path planner that connects waypoints to form a time-dependent trajectory that can be tracked by vehicles with first-order nonholonomic constraints with guaranteed asymptotic convergence.

The remainder of this paper begins in Section 2 by outlining the necessary background for the development of the proposed zero-error ϵ -trajectory tracking. Section 3 presents the main result of the paper: error-free trajectory tracking accomplished by redefining an arbitrary reference trajectory in terms of the ϵ -point. Section 4 presents an example application by extending continuous curvature paths to trajectories and using the ϵ -trajectory tracking method to follow a desired trajectory. The paper ends with concluding remarks in Section 5.

2 Preliminaries

This section presents the preliminary information necessary to understand the contributions of this work. The motion models used for vehicle control and analysis are first developed, followed by an introduction to the ϵ -point control. This section ends with a discussion of the CCPaths.

2.1 Kinematic Models

Four kinematic models are presented in this section. The first two describe the vehicle motion models being controlled, the third describes a model used to create trajectories, and the last is a model used solely for convergence analysis. The simplest model to be employed is the unicycle model. It is a model of a first-order nonholonomic constrained system that can be represented as

$$\begin{bmatrix} \dot{x} \\ \dot{y} \\ \dot{\psi} \\ \dot{v} \\ \dot{\omega} \end{bmatrix} = \begin{bmatrix} v \cos \psi \\ v \sin \psi \\ \omega \\ 0 \\ 0 \end{bmatrix} + \begin{bmatrix} 0 & 0 \\ 0 & 0 \\ 0 & 0 \\ 1 & 0 \\ 0 & 1 \end{bmatrix} \begin{bmatrix} a \\ \alpha \end{bmatrix}, \quad (1)$$

where (x, y) is the position of the robot, ψ is the heading, v is the translational velocity, ω is the rotational velocity, and a and α are the longitudinal and angular acceleration, respectively, e.g. [11]. The positions, velocities, and accelerations can be grouped together as $\underline{x} = [x, y]^T$, $\underline{v} = [v, \omega]^T$, and $\underline{a} = [a, \alpha]^T$. The first two rows in (1) describe the lateral motion constraint of a wheeled vehicle. As a result, more complex kinematic models can be related to (1) using algebraic mappings [11].

One such model that will be used is the Ackermann-style bicycle model [19]. It represents the lateral motion constraint as in (1) with the angular velocity being a function of the steering angle and longitudinal velocity to present a more realistic input for steered vehicles. It can be represented as

$$\begin{bmatrix} \dot{x} \\ \dot{y} \\ \dot{\psi} \\ \dot{v} \\ \dot{\phi} \end{bmatrix} = \begin{bmatrix} v \cos \psi \\ v \sin \psi \\ \frac{v}{L} \tan \phi \\ 0 \\ 0 \end{bmatrix} + \begin{bmatrix} 0 & 0 \\ 0 & 0 \\ 0 & 0 \\ 1 & 0 \\ 0 & 1 \end{bmatrix} \begin{bmatrix} a \\ \xi \end{bmatrix}, \quad (2)$$

where ϕ is the steering angle, L is the wheelbase, and ξ is the steering rate, as seen in Figure 1. This model is used in many kinematic controllers because ξ can be directly related to a steering wheel input.

The extended Dubins model, which was initially introduced in [3] to explore the distance optimal path for trajectories in \mathbb{C}^2 , where \mathbb{C}^k denotes the set of functions which are k times continuously differentiable, proves useful for creating trajectories which respect the curvature constraints of the system. It can again be seen as an extension to (1) where the angular velocity is calculated in terms of the curvature

as follows

$$\begin{bmatrix} \dot{x} \\ \dot{y} \\ \dot{\psi} \\ \dot{\kappa} \end{bmatrix} = \begin{bmatrix} v \cdot \cos \psi \\ v \cdot \sin \psi \\ v \cdot \kappa \\ 0 \end{bmatrix} + \begin{bmatrix} 0 \\ 0 \\ 0 \\ 1 \end{bmatrix} \sigma, \quad (3)$$

where κ is curvature and σ is the change in curvature. There are no dynamics for v as it is assumed constant.

To prove convergence of the ϵ -tracking algorithm, a trailer model will be used. The trailer model can be viewed as an extension to (1) where a trailer is connected via a hitch to the rear axle, as depicted in Figure 1. The trailer model is given by

$$\begin{bmatrix} \dot{x} \\ \dot{y} \\ \dot{\psi} \\ \dot{\psi}_t \\ \dot{v} \\ \dot{\omega} \end{bmatrix} = \begin{bmatrix} v \cos \psi \\ v \sin \psi \\ \omega \\ \frac{v}{d} \sin(\psi - \psi_t) \\ 0 \\ 0 \end{bmatrix} + \begin{bmatrix} 0 & 0 \\ 0 & 0 \\ 0 & 0 \\ 0 & 0 \\ 1 & 0 \\ 0 & 1 \end{bmatrix} \begin{bmatrix} a \\ \alpha \end{bmatrix} \quad (4)$$

where ψ_t is the heading of the trailer, and d is the length of the hitch (e.g. [16]). Note that the position of the trailer can be directly computed from \underline{x} , d , and ψ_t and is therefore not included as a state in (4).

2.2 Tracking Methods

With the kinematic models to be controlled in hand, our attention now turns to the point-control laws that will be extended to provide exact tracking of a desired trajectory. A myriad of control approaches have been used for tracking a desired path such as utilizing approximate linearization [5], sinusoid control inputs [16], vector field following [9], or other nonlinear control laws [8, 20, 21] to name a few.

This section focuses on the approach developed by Olfati-Saber as it provides a framework to directly deal with the nonholonomic constraints in wheeled vehicles by focusing on a point directly in front of the vehicle, a point referred to as the ϵ -point [17]. This is, of course, not the only method that has used a point in front of the vehicle for the basis of control. For example, the pure-pursuit method [2, 4] uses a look-ahead point to connect the vehicle to the desired path using a proportional curvature controller. As the look-ahead point increases, the robot experiences greater stability but results in steady-state errors and requires tuning for different speeds [18]. The ϵ -point tracking introduced by Olfati-Saber has a similar steady-state error trend without the need for extensive tuning due to the global exponential stability guarantees.

In what follows, a simplified version of the control presented by Olfati-Saber is presented that allows for partial feedback linearization. The results of this section can be derived from the results in [17] and are presented for the sake of clarity in understanding both the notation and contributions of future sections. The simplification of this section with respect to [17] is that ϵ is maintained constant whereas, in [17], ϵ decreases to an arbitrarily small value. Theoretically, this arbitrary smallness is beneficial for tracking a trajectory; practically, disturbances pose issues for implementation.

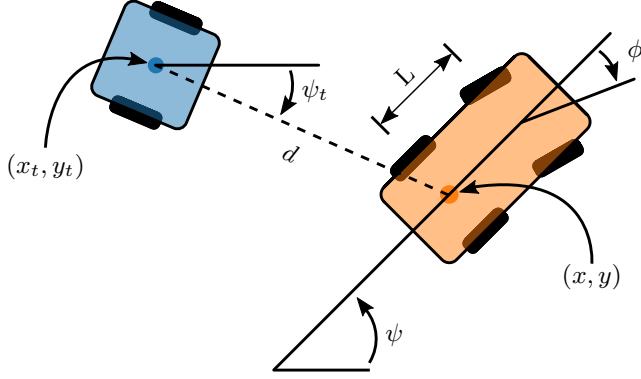


Fig. 1: Dynamics of a car pulling a trailer where L is the wheelbase, ϕ is the steering angle of the pulling vehicle, and d is the length of the hitch between the connected trailer and the pulling vehicle. The angular velocity of the pulling vehicle can be computed using ϕ and L where $\omega = \frac{v}{L} \tan \phi$.

Consider a point $\mathbf{q} = [x, y]^T \in \mathbb{R}^2$ where $\ddot{\mathbf{q}}$ is the control input to the system. Let $\mathbf{p} = [\mathbf{q}, \dot{\mathbf{q}}]^T$. The dynamics of the point can be written as

$$\dot{\mathbf{p}} = \mathbf{A}\mathbf{p} + \mathbf{B}\mathbf{u} = \begin{bmatrix} \mathbf{0} & \mathbf{I} \\ \mathbf{0} & \mathbf{0} \end{bmatrix} \begin{bmatrix} \mathbf{q} \\ \dot{\mathbf{q}} \end{bmatrix} + \begin{bmatrix} \mathbf{0} \\ \mathbf{I} \end{bmatrix} \mathbf{u} \quad (5)$$

where \mathbf{I} is the 2×2 identity matrix and $\mathbf{0}$ is a 2×2 matrix of zeros. Given the proposed system, the point \mathbf{p} exponentially tracks a reference trajectory per the following lemma.

Lemma 1 *Given the system defined in (5), let $\mathbf{q}_r = [x_r, y_r]^T \in \mathbb{C}^2$, $\mathbf{p}_r = [\mathbf{q}_r, \dot{\mathbf{q}}_r]^T$ and $\mathbf{u} = \ddot{\mathbf{x}}_r - K(\mathbf{p} - \mathbf{p}_r)$, with the real parts of the eigenvalues of $\mathbf{A} - \mathbf{B}K$ being negative, then $\mathbf{q}(t)$ is globally exponentially stable to $\mathbf{x}_r(t)$.*

Proof Let an error state \mathbf{z} be introduced where $\mathbf{z} = \mathbf{p} - \mathbf{p}_r$. Defining $\mathbf{u} = -K\mathbf{z} + \ddot{\mathbf{q}}_r$, the time derivative of \mathbf{z} can be written as $\dot{\mathbf{z}} = (\mathbf{A} - \mathbf{B}K)\mathbf{z}$. It can be verified that (\mathbf{A}, \mathbf{B}) forms a completely controllable linear time-invariant system which completes the proof.

Lemma 1 cannot be directly applied to the unicycle model as the inputs and dynamics are obviously not matched. However, \mathbf{q}_ϵ can be defined as a point directly in front of the vehicle such that

$$\mathbf{q}_\epsilon = \begin{bmatrix} x \\ y \end{bmatrix} + \epsilon \begin{bmatrix} \cos \psi \\ \sin \psi \end{bmatrix} \quad (6)$$

where $\epsilon > 0$ is constant. The point \mathbf{q}_ϵ can then be defined so that it behaves as if it were the constraint-free point in Lemma 1 using an algebraic relationship between \mathbf{u} in Lemma 1 and the control inputs in (1). This relationship is stated in the following lemma.

Lemma 2 Let $\underline{x}_r = [x_r, y_r]^T \in \mathbb{C}^2$ be a reference trajectory for a vehicle with unicycle dynamics as defined in (1). Let \underline{u}_ϵ be defined as the control input to the point system from Lemma 1. Define the system input as:

$$\underline{a} = R_\epsilon^{-1} \underline{u}_\epsilon - \hat{\omega} \underline{v}. \quad (7)$$

where

$$R_\epsilon^{-1} = \begin{bmatrix} \cos \psi & -\frac{1}{\epsilon} \sin \psi \\ \sin \psi & \frac{1}{\epsilon} \cos \psi \end{bmatrix} \quad (8)$$

then $\underline{q}_\epsilon(t) \rightarrow \underline{x}_r(t)$ globally and exponentially fast.

Proof The first and second derivatives for \underline{q}_ϵ can be directly calculated and written as:

$$\dot{\underline{q}}_\epsilon = R_\epsilon \underline{v}, \quad (9)$$

$$\ddot{\underline{q}}_\epsilon = R_\epsilon \hat{\omega} \underline{v} + R_\epsilon \underline{a} \quad (10)$$

$$R_\epsilon = \begin{bmatrix} \cos \psi & -\epsilon \sin \psi \\ \sin \psi & \epsilon \cos \psi \end{bmatrix}, \quad \hat{\omega} = \begin{bmatrix} 0 & -\epsilon \omega \\ \frac{\omega}{\epsilon} & 0 \end{bmatrix}. \quad (11)$$

Therefore, by setting $\ddot{\underline{q}}_\epsilon$ equal to \underline{u}_ϵ and algebraically solving for \underline{a} , the dynamics for $\underline{q}_\epsilon(t)$ are matched to (5), and $\underline{q}_\epsilon(t) \rightarrow \underline{x}_r(t)$ globally and exponentially fast, per Lemma 1.

Corollary 1 Due to Lemma 2, $\|\underline{e}(t)\| \rightarrow \epsilon$ where $\underline{e} = \underline{x} - \underline{x}_r$.

This corollary can be seen by noting that the ϵ -point converges to \underline{x}_r and, by definition, \underline{x} is a distance ϵ from the \underline{q}_ϵ .

Lemma 2 can be directly extended to the bicycle model in (2) by forming one additional algebraic relationship which relates the steering input of the bicycle to the angular acceleration input of the unicycle. A small contribution to ϵ -tracking is now made by extending it to the bicycle model in (2), as shown in Figure 2. In the bicycle model, the angular velocity is given by $\omega = \frac{v}{L} \tan \phi$. By differentiating the angular velocity, the angular acceleration can be written as:

$$\alpha = \frac{a}{L} \cdot \tan(\phi) + \frac{v}{L} \cdot \frac{\xi}{\cos^2(\phi)}. \quad (12)$$

Rearranging terms, the steering input can be expressed as:

$$\xi = \frac{1}{v} \cos^2(\phi) (L\alpha - a \cdot \tan(\phi)). \quad (13)$$

Thus, given the inputs \underline{a} in Lemma 2, the inputs to the bicycle, (a, ξ) , can be directly computed as long as $v \neq 0$.

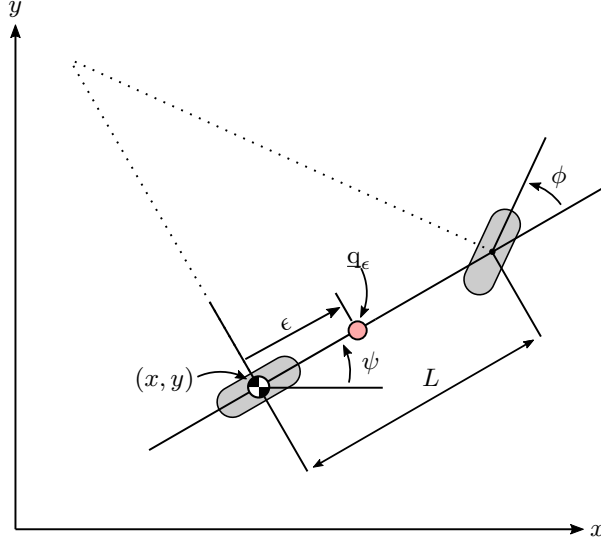


Fig. 2: Proposed control reference point \mathbf{q}_ϵ used to linearize the bicycle model.

2.3 Continuous Curvature Paths

The CCPath was first introduced by Fraichard and Scheuer to plan a path that accounts for the maximum curvature and maximum change in curvature [7]. This allows for planning paths that consider fundamental vehicle execution constraints or even, as shown in [22], to adhere to passenger acceleration and jerk constraints. A CCPath is formed by connecting two oriented waypoints using straight lines, circular arcs, and transition arcs as seen in Figure 3.

The transition arcs are formed by generating a Clothoid, also referred to as the Euler Spiral, which is defined as a path whose curvature increases linearly with arc length [13]. Because the Clothoid produces continuous curvature paths, it approximates the kinematic curvature limitations imposed by physical actuators on mobile robots [15]. The parametric equations to form a Clothoid are referred to as the Fresnel integral and are represented as

$$\begin{aligned} x = C_f &= x_0 + \int_0^s \cos\left(\frac{1}{2}\sigma(\xi^2 + \kappa_0\xi + \psi_0)\right) d\xi \\ y = S_f &= y_0 + \int_0^s \sin\left(\frac{1}{2}\sigma(\xi^2 + \kappa_0\xi + \psi_0)\right) d\xi \end{aligned} \quad (14)$$

where (x, y) is the position, ψ is the heading, κ is curvature, and σ is the change in curvature [12].

The general case for a turn in a CCPath is referred to as a continuous curvature turn (CCTurn) which is composed of three stages for both positive and negative velocity: (1) a transition arc of linearly changing curvature from 0 to $\pm\kappa_{\max}$ at a rate of $\pm\sigma_{\max}$, where κ_{\max} is the maximum allowable curvature and σ_{\max} is

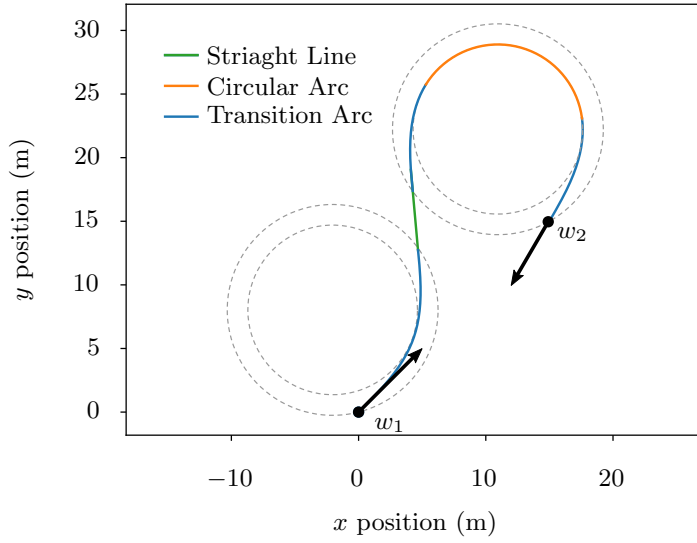


Fig. 3: Connecting directional waypoints w_1 and w_2 using straight lines, circular arcs, and transition arcs composed of Clothoids.

the maximum allowable change in curvature, (2) a circular arc with a constant curvature of $\pm\kappa_{\max}$, and (3) a transition arc of linearly changing curvature from $\pm\kappa_{\max}$ to 0 at a rate of $\pm\sigma_{\max}$ [7].

One difficulty of path-following controllers for CCPaths is determining which point on the path to follow. This can be done by finding the closest lateral point on the path, often referred to as the cross-track error. Calculating cross-track error introduces new complexities including how to optimally calculate or measure cross-track error, and how to avoid errors originating from self-intersecting paths [9]. Following a time-indexed path (referred to as a trajectory) largely eliminates this difficulty by using a time-index to determine the point to follow. Note the similarity of (14) to the unicycle model in (1). The evolution of x depends on the cosine of some changing value and the evolution of y likewise depends on the sine. This will be exploited in Section 4 to create a natural time-indexing of a CCPath based on the kinematic constraints of a vehicle.

3 Zero-Error ϵ -Trajectory Tracking

This section uses the ϵ -tracking method to achieve zero-error ϵ -trajectory tracking by creating a trajectory that, when tracked by the ϵ -point, results in perfect tracking of the original trajectory by the robot. The formation of the new trajectory is addressed in Section 3.1 and Section 3.2 analyzes the stability properties of tracking the new trajectory using ϵ -tracking.

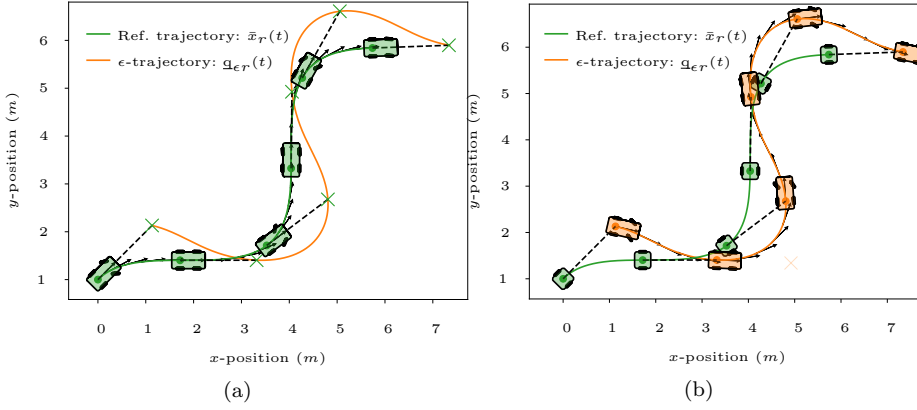


Fig. 4: (a) Depiction of the generation of an ϵ -trajectory from the point $\mathbf{q}_{\epsilon r}$, which leads the reference trajectory by a distance of ϵ . (b) Representation of the vehicle reference point acting as a trailer being pulled by the ϵ -trajectory.

3.1 Generating an ϵ -Trajectory

It was shown in Lemma 2 that ϵ -tracking produces a steady-state error equal to the length of ϵ . To eliminate the steady-state error, this section develops a method to exploit the knowledge of the desired trajectory and vehicle dynamics to generate a new trajectory that is intended for the control point used in ϵ -tracking. The new trajectory is referred to as an ϵ -trajectory because it is generated for the ϵ -point.

Let $\underline{x}_r = [x_r, y_r]^T \in \mathbb{C}^2$ be a reference trajectory intended for execution by a unicycle in (1). Appendix A derives the states and inputs of the unicycle model to achieve perfect tracking without disturbances such that:

$$\begin{aligned}
 \psi_r &= \text{atan2}(\dot{y}_r, \dot{x}_r) \\
 v_r &= \sqrt{\dot{x}_r^2 + \dot{y}_r^2} \\
 a_r &= (\dot{x}_r \ddot{x}_r + \dot{y}_r \ddot{y}_r) v_r^{-1} \\
 \omega_r &= (\dot{x}_r \ddot{y}_r - \dot{y}_r \ddot{x}_r) v_r^{-2} \\
 \alpha_r &= (\dot{x}_r \ddot{\ddot{y}}_r - \dot{y}_r \ddot{\ddot{x}}_r) v_r^{-2} - 2a_r \omega_r v_r^{-1}
 \end{aligned} \tag{15}$$

Note that if the vehicle were to achieve perfect tracking, the ϵ -point would be located at a distance of ϵ in front of the vehicle, as depicted in Figure 4 (a). Figure 4 (a) shows a vehicle driving a cosine trajectory, and the ϵ -trajectory is depicted as the point leading the trajectory.

Thus, the ϵ -trajectory, denoted $\mathbf{q}_{\epsilon r}$, is defined in terms of the reference position and orientation as:

$$\mathbf{q}_{\epsilon r} = \begin{bmatrix} x_{\epsilon r} \\ y_{\epsilon r} \end{bmatrix} = \begin{bmatrix} x_r \\ y_r \end{bmatrix} + \epsilon \begin{bmatrix} \cos \psi_r \\ \sin \psi_r \end{bmatrix}. \tag{16}$$

Subsequent derivatives can then be taken of $\mathbf{q}_{\epsilon r}$ so that the controller presented in the sequel can track $\mathbf{q}_{\epsilon r}$. The first and second derivatives of $\mathbf{q}_{\epsilon r}$ can be stated

as

$$\begin{aligned}\dot{\mathbf{q}}_{\epsilon r} &= R_{\epsilon r} \mathbf{v}_r \\ \ddot{\mathbf{q}}_{\epsilon r} &= R_{\epsilon r} \dot{\omega}_r \mathbf{v}_r + R_{\epsilon r} \mathbf{a}_r\end{aligned}\tag{17}$$

where matrices are defined equivalently to (11). Though not necessary for trajectory tracking, the relationship between the ϵ -trajectory and the reference trajectory can be viewed as a vehicle pulling a trailer instead of a point leading a vehicle, as depicted in Figure 4 (b). Figure 4 (b) shows that the ϵ -trajectory can be represented as a vehicle with a heading and velocities calculated similar to (15) and written as:

$$\begin{aligned}\psi_{\epsilon r} &= \text{atan2}(\dot{y}_{\epsilon r}, \dot{x}_{\epsilon r}) \\ v_{\epsilon r} &= \sqrt{\dot{x}_{\epsilon r}^2 + \dot{y}_{\epsilon r}^2} \\ \omega_{\epsilon r} &= (\dot{x}_{\epsilon r} \ddot{y}_{\epsilon r} - \dot{y}_{\epsilon r} \ddot{x}_{\epsilon r}) v_{\epsilon r}^{-2}\end{aligned}\tag{18}$$

This relationship is significant because it is used to prove convergence in the following section, and it provides additional intuition as to how the length of ϵ and velocity of the trajectory affect the speed of convergence.

3.2 Stability of Zero-Error ϵ -Trajectory Tracking

With a modified trajectory for the ϵ -point in hand, this section presents a theorem and proof showing that using the ϵ -tracking controller to follow the ϵ -trajectory will cause the vehicle reference point to converge to the original reference trajectory. The proof of the result can intuitively be thought of in two parts: a driving phase and a pulling phase, as depicted in Figure 5 (a). In the driving phase, the ϵ -point converges to the ϵ -trajectory according to the gains of the control law proposed in Lemma 1. The driving phase is depicted in Figure 5 (a) as the ϵ -point aggressively connects to the ϵ -trajectory, wherein the pulling phase is entered¹. In the pulling phase, the vehicle reference point and the reference trajectory follow the ϵ -trajectory at a fixed distance of ϵ , and therefore behave as two trailers being pulled by a single vehicle with a hitch at $\mathbf{q}_{\epsilon r}$. This relationship is depicted in Figure 5 (b) where the vehicle reference point and reference trajectory are shown as two trailers being pulled by the ϵ -trajectory.

The movement of the “trailers” are analyzed, and it is shown that the vehicle asymptotically converges to the desired trajectory. These phases are mirrored in the proof where Lemma 2 is used to show the convergence of the ϵ -point, and LaSalle’s invariance principle [10] is used to evaluate the invariant set consisting of the allowable states once the driving phase has “completed”.

The dynamic equations for a vehicle pulling two trailers at a distance of ϵ can be expressed using (4) by adding an additional trailer heading and substituting ϵ

¹ Note that there is no physical switching between the two phases, as both phases occur simultaneously to produce asymptotic convergence

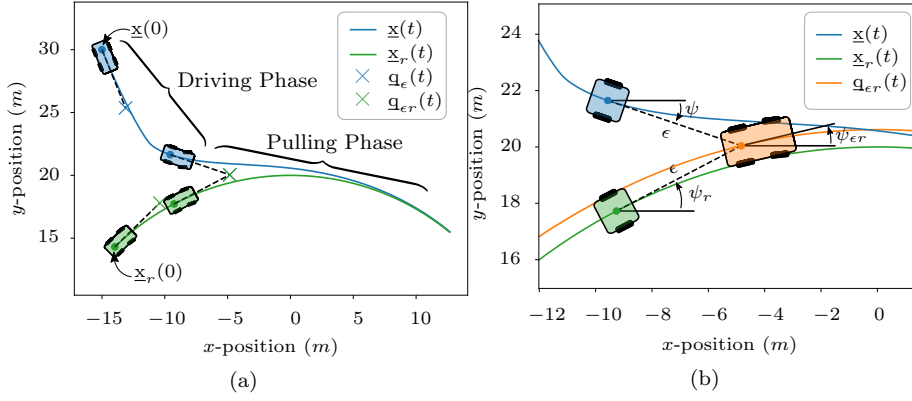


Fig. 5: (a) Representation of the driving and pulling phases, where the blue and green vehicles represent discrete time intervals of \underline{x} and \underline{x}_r respectively. The driving phase dominates as \underline{q}_ϵ converges exponentially fast to $\underline{q}_{\epsilon r}$ as shown in Lemma 2, and the pulling phase dominates as $\underline{q}_\epsilon(t) \rightarrow \underline{q}_{\epsilon r}(t)$. (b) Zoomed in illustration of Figure 5 a during the pulling phase, which depicts the control system as two trailers being pulled by the ϵ -trajectory. As $\underline{q}_\epsilon(t) \rightarrow \underline{q}_{\epsilon r}(t)$ each system follows the ϵ -trajectory by a fixed value of ϵ just as trailers are pulled behind a vehicle by a hitch.

for d . Expressed in terms of the ϵ -trajectory, this can be described as:

$$\begin{bmatrix} \dot{x}_{\epsilon r} \\ \dot{y}_{\epsilon r} \\ \dot{\psi}_{\epsilon r} \\ \dot{\psi} \\ \dot{\psi}_r \\ \dot{v}_\epsilon \\ \dot{\omega}_\epsilon \end{bmatrix} = \begin{bmatrix} v_{\epsilon r} \cos(\psi_{\epsilon r}) \\ v_{\epsilon r} \sin(\psi_{\epsilon r}) \\ \omega_\epsilon \\ \frac{v_{\epsilon r}}{\epsilon} \sin(\psi_{\epsilon r} - \psi) \\ \frac{v_{\epsilon r}}{\epsilon} \sin(\psi_{\epsilon r} - \psi_r) \\ 0 \\ 0 \end{bmatrix} + \begin{bmatrix} 0 & 0 \\ 0 & 0 \\ 0 & 0 \\ 0 & 0 \\ 0 & 0 \\ 1 & 0 \\ 0 & 1 \end{bmatrix} \begin{bmatrix} a_\epsilon \\ \alpha_\epsilon \end{bmatrix} \quad (19)$$

where the definitions for the variables in (19) are listed in Table 1 and the two-trailer relationship is depicted in Figure 5 (b). The main result for convergence is presented in the following theorem:

Theorem 1 Let \underline{x}_r be a reference trajectory defined for $t \geq 0$, then $\underline{x}(t)$ will asymptotically converge to $\underline{x}_r(t)$ under the following assumptions:

- i) $\underline{x}_r \in \mathbb{C}^2$
- ii) $v_r > 0$ as calculated in (15)
- iii) $q_{\epsilon r}$ is defined as in (15) and (17)
- iv) The vehicle dynamics are algebraically mapped to the unicycle model
- v) The control law from Lemma 2 is applied using $q_{\epsilon r}$ as a reference trajectory

Proof Lemma 2 can be invoked to show that $\underline{q}_\epsilon(t) \rightarrow \underline{q}_{\epsilon r}(t)$ at an exponential rate. Due to LaSalle's invariance principle, we need only evaluate the evolution of the state in the invariant set. In the invariant set,

$$\mathbf{0} = \underline{q}_\epsilon - \underline{q}_{\epsilon r}. \quad (20)$$

Table 1: Descriptions for frequently used variables.

Variable	Description
\underline{x}	Vehicle position
\underline{q}_ϵ	ϵ -control point in front of \underline{x}
\underline{x}_r	Reference trajectory position
$\underline{q}_{\epsilon r}$	ϵ -trajectory point in front of \underline{x}_r
ϵ	Distance from vehicle to control-reference point
ψ	Heading of vehicle
ψ_r	Heading of reference trajectory
$\psi_{\epsilon r}$	Heading of ϵ -trajectory
$v_{\epsilon r}$	Longitudinal velocity of ϵ -trajectory
$\omega_{\epsilon r}$	Angular velocity of the ϵ -trajectory
$a_{\epsilon r}$	Longitudinal acceleration of ϵ -trajectory
$\alpha_{\epsilon r}$	Anglar acceleration of ϵ -trajectory

Defining $\underline{e} = \underline{x}_r - \underline{x}$, (20) can be re-arranged to obtain

$$\underline{e} = \begin{bmatrix} \epsilon (\cos \psi_r - \cos \psi) \\ \epsilon (\sin \psi_r - \sin \psi) \end{bmatrix}. \quad (21)$$

To show that $\underline{e}(t) \rightarrow 0$ in the invariant set, consider the state $e = \psi - \psi_r$. The time derivative of e can be written using (19) as

$$\dot{e} = -\frac{v_{\epsilon r}}{\epsilon} (\sin(\psi_{\epsilon r} - \psi_r) - \sin(\psi_{\epsilon r} - \psi)), \quad (22)$$

where $e \in [-\pi, \pi)$. Consider the Lyapunov candidate function

$$V = \frac{1}{2}e^2. \quad (23)$$

The derivative for V can be expressed as

$$\dot{V} = e\dot{e} = -\frac{v_{\epsilon r}}{\epsilon}e (\sin(\psi_{\epsilon r} - \psi_r) - \sin(\psi_{\epsilon r} - \psi)). \quad (24)$$

Appendix B shows that

$$\text{sign}(e) = \text{sign}(\sin(\psi_{\epsilon r} - \psi_r) - \sin(\psi_{\epsilon r} - \psi)) \quad (25)$$

when $|\psi_{\epsilon r} - \psi| < \frac{\pi}{2}$. Since $v_{\epsilon r}$ and ϵ are strictly positive, this implies (24) is negative definite when $|\psi_{\epsilon r} - \psi| < \frac{\pi}{2}$. Therefore, $\psi(t) \rightarrow \psi_r(t)$ and $\underline{e}(t) \rightarrow 0$ asymptotically.

4 Waypoint Trajectory Planning and Following

As mentioned in the introduction, CCPaths are an established method to plan paths that honor the curvature constraints of a wheeled vehicle. To demonstrate the utility of the trajectory following controller developed in previous sections, we present an extension of adding a time index to CCPaths, and we call the

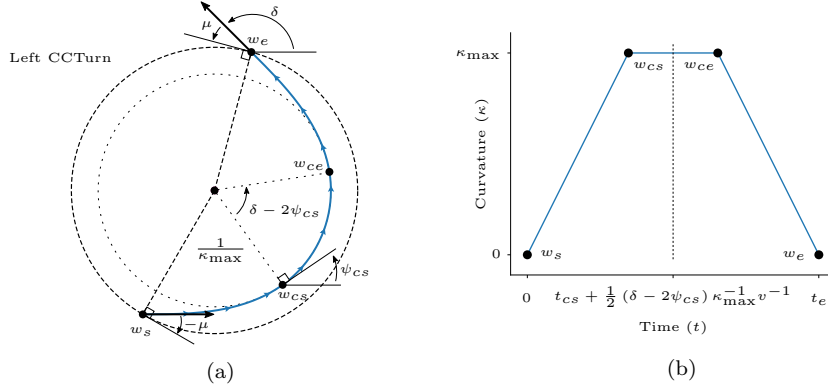


Fig. 6: It should be noted that though this figure is of a left turn starting with zero initial conditions, it can easily be extended to any translation or rotation and mirrored across the x -axis to represent a right turn. (a) Figure depicting the generation of a time-dependent CCTurn trajectory that achieves a change in heading of δ radians from starting at w_s and ending at w_e . (b) Plot demonstrating the curvature continuity of a CCTurn as a function of time where t_e represents the end time at the point w_e . Note that the curvature profile is mirrored across the midpoint of time.

result a continuous curvature trajectory (CCTrajectory). Thus, a CCTrajectory is a time indexed CCPath with a fixed positive velocity that connects two oriented waypoints by concatenating turns of maximum change in curvature, referred to as CCTurns, with straight line segments as depicted in Figure 3. The planning of arcs and lines in a CCTrajectory is performed in the same way as a CCPath. As a result, the reader is referred to [7] for planning details, and the following is focused on CCTurns generation.

Figure 6 shows how a time-dependent CCTurn is developed using transition-arcs, circular-arcs, and linear paths to achieve a desired change in heading. A CCTurn consists of four oriented waypoints (w_s , w_{cs} , w_{ce} , w_e) which create a change of heading equal to δ , in the following three segments:

1. Change from zero curvature to maximum curvature (w_s to w_{cs})
2. Constant curvature arc (w_{cs} to w_{ce})
3. Change from maximum curvature to zero curvature (w_{ce} to w_e)

where each waypoint consists of a position, orientation, starting curvature, and linear change in curvature. In the following descriptions, the time-indexing of each segment required to build a CCTrajectory is explained in terms of the states in (3), which are used to calculate the position derivatives of the trajectory.

Change to Maximum Curvature

To generate a time-dependent transition-arc trajectory from w_s to w_{cs} the model (3) is integrated instead of using (14) to produce a Clothoid. Integrating (3) to obtain a transition arc ensures that the spacing between points is consistent with the vehicle's desired velocity, and it produces the necessary states at each point to

solve for the position derivatives used for vehicle control. The CCTurn starts at w_s with zero curvature, and it turns with the maximum change in curvature until $\kappa = \kappa_{\max}$. The corresponding waypoints for the segment w_s and w_{cs} are

$$w_s = \begin{cases} x_s &= 0 \\ y_s &= 0 \\ \psi_s &= 0 \\ \kappa_s &= 0 \\ \sigma_s &= \sigma_{\max} \end{cases}, \quad w_{cs} = \begin{cases} x_{cs} &= \int_0^{t_{cs}} v \cos(\psi(t)) dt \\ y_{cs} &= \int_0^{t_{cs}} v \sin(\psi(t)) dt \\ \psi_{cs} &= \int_0^{t_{cs}} v \kappa(t) dt \\ \kappa_{cs} &= \kappa_{\max} \\ \sigma_{cs} &= 0 \end{cases} \quad (26)$$

where the time at w_{cs} is $t_{cs} = v \frac{\kappa_{\max}}{\sigma_{\max}}$, and v is a constant desired velocity.

Constant Curvature Arc

After the trajectory reaches maximum curvature, it begins the creation of a circular arc at the point w_{cs} . To generate a time-dependent circular arc (the region between w_{cs} and w_{ce} in Figure 6), it is unnecessary to integrate (3) to obtain the trajectory position because the closed-form equation of a circular arc exists. The distance between points can be analytically computed on the perimeter of the circular arc as

$$ds = v \cdot dt \quad (27)$$

where dt is the discrete-time integration step, and the total circular-arc length becomes

$$s = (\delta - 2\psi_{cs}) \kappa_{\max}^{-1}. \quad (28)$$

Though (3) does not need to be integrated to obtain the position states of the circular trajectory, it can be used to solve the other system states at each point. The system states for every index on the circular arc are

$$\begin{aligned} \psi(t) &= \psi_c(t) + d_c \frac{\pi}{2} \\ \kappa(t) &= \kappa_{\max}, \quad \sigma(t) = 0 \\ v(t) &= \text{const}, \quad \alpha(t) = 0 \end{aligned} \quad (29)$$

where ψ_c is the angle of the zero motion line referenced from the instantaneous center of rotation and d_c is the vehicle's direction of motion such that a clockwise rotation is $d_c = 1$ and a counterclockwise rotation is $d_c = -1$.

Change to Zero Curvature

As for generating the second transition arc on the CCTurn from w_{ce} to w_e , it can be computed by again integrating (3) starting with a curvature of κ_{\max} and decreasing the curvature at the maximum rate until it reaches 0. Equation (26) can be used in reverse as the second transition arc is a mirror image of the first.

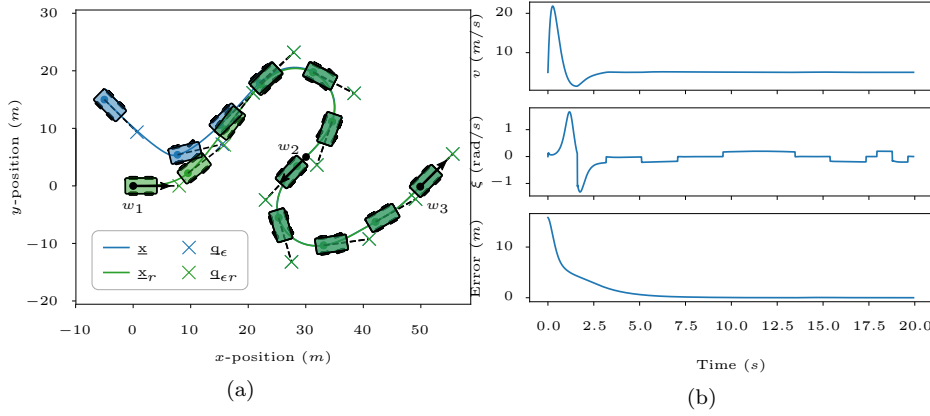


Fig. 7: (a) Deomonstration of zero-error ϵ -trajectory tracking showing that the vehicle \underline{x} asymptotically converges to \underline{x}_r , where \underline{x}_r is a CCTrajectory that passes through the waypoints w_1 , w_2 , and w_3 . (b) Analysis of the system velocity v , steering rate input ξ , and position error between \underline{x} and \underline{x}_r during the demonstration of zero-error ϵ -trajectory tracking.

Finally, to generate a time-dependent linear trajectory used to connect two CCTurns, no integration is necessary. The distance between each point on the line is equal to (27), and the corresponding system states are

$$\begin{aligned}\psi(t) &= \text{atan2}(p_{2y} - p_{1y}, p_{2x} - p_{1x}) \\ \kappa(t) &= 0, \sigma = 0 \\ v(t) &= \text{const}, \alpha = 0\end{aligned}\tag{30}$$

such that $p_1 = [p_{1x}, p_{1y}]^T$ and $p_2 = [p_{2x}, p_{2y}]^T$ are the points that linearly connect two CCTurns. After the pieces of the CCTrajectory are generated, they are concatenated to make a continuous trajectory, and the position derivatives of the reference trajectory are obtained by differentiating x and y from (3).

4.1 Simulation Results

An example is now presented to demonstrate zero-error ϵ -trajectory tracking of a CCTrajectory. The example uses a value of $\epsilon = 5\text{ m}$ to slow the convergence of the pulling phase for the sake of illustration but in practice the value of ϵ is system dependent. The scenario uses a CCTrajectory with a velocity of 5 m/s and three waypoints of the form $\omega_i = [x_i, y_i, \psi_i]^T$ where (x_i, y_i) is the position, and ψ is the heading of the waypoint ω_i . The waypoints are located at $w_1 = [0, 0, 0]$, $w_2 = [30, 5, \frac{5\pi}{4}]$, and $w_3 = [50, 0, \frac{\pi}{4}]$. Figure 7 (a) shows the path connection between the points with a $\kappa_{\max} = \pm 2.7\text{ m}^{-1}$ and $\sigma_{\max} = \pm 0.17\text{ (ms)}^{-1}$. Figure 7 (b) shows the convergence to zero-error tracking.

5 Conclusion

In this paper, a controller for kinematic vehicles with acceleration inputs and first-order nonholonomic constraints has been presented that results in zero-error trajectory tracking. The controller uses partial feedback linearization to control a new reference point in front of the vehicle's rear axle. However, controlling a new reference point results in a steady-state error between the original reference point and the desired reference trajectory. Therefore, the generation of a new trajectory is proposed that when tracked by the new reference point, results in zero-error vehicle tracking of the original reference trajectory. It is proven that any trajectory that is twice differentiable guarantees zero-error tracking using the proposed controller when the vehicle is at least within $\pm \frac{\pi}{2}$ radians of the direction of the new trajectory. This paper further demonstrated how to generate time-dependent, continuous curvature trajectories that connect waypoints, given a maximum curvature and change in curvature. The presented controller is proven to asymptotically track these trajectories, and the results are demonstrated through simulation.

References

1. Aguiar, A.P., Hespanha, J.P., Kokotovic, P.V.: Path-following for nonminimum phase systems removes performance limitations. *IEEE Transactions on Automatic Control* **50**(2), 234–239 (2005). DOI 10.1109/TAC.2004.841924
2. Amidi, O.: *Integrated Mobile Robot Control*. Robotics Institute, Pittsburgh, PA (1990)
3. Boissonnat, J.D., Cerezo, A., Leblond, J., Robotique, P., Prisme, P.: A note on shortest paths in the plane subject to a constraint on the derivative of the curvature (1994)
4. Coulter, R.C.: Implementation of the pure pursuit path tracking algorithm. Tech. Rep. CMU-RI-TR-92-01, Carnegie Mellon University, Pittsburgh, PA (1992)
5. De Luca, A., Oriolo, G., Samson, C., Laumond, J.P.: Feedback Control of a Nonholonomic Car-like Robot Robot Motion Planning and Control Feedback Control of a Nonholonomic Car-Like Robot. Tech. rep. (1998)
6. Dubins, L.E.: On Curves of Minimal Length with a Constraint on Average Curvature, and with Prescribed Initial and Terminal Positions and Tangents. *American Journal of Mathematics* (1957). DOI 10.2307/2372560
7. Fraichard, T., Scheuer, A.: From Reeds and Shepp's to continuous-curvature paths. *IEEE Transactions on Robotics* (2004). DOI 10.1109/TRO.2004.833789
8. Hoffmann, G.M., Tomlin, C.J., Montemerlo, M., Thrun, S.: Autonomous automobile trajectory tracking for off-road driving: Controller design, experimental validation and racing. In: *Proceedings of the American Control Conference* (2007). DOI 10.1109/ACC.2007.4282788
9. Kapitanyuk, Y.A., Proskurnikov, A.V., Cao, M.: A Guiding Vector-Field Algorithm for Path-Following Control of Nonholonomic Mobile Robots. *IEEE Transactions on Control Systems Technology* **26**(4), 1372–1385 (2018). DOI 10.1109/TCST.2017.2705059
10. LaSalle, J., Lefschetz, S.: *Stability by Liapunov's direct method: with applications*. Mathematics in science and engineering. Academic Press (1961)
11. LaValle, S.M.: Planning algorithms. *Planning Algorithms* **9780521862**, 1–826 (2006). DOI 10.1017/CBO9780511546877
12. Lekkas, A.M.: Anastasios M. Lekkas Guidance and Path-Planning Systems for Autonomous Vehicles (2014)
13. Levién, R.: *The euler spiral: A mathematical history*. Berkeley, CA (2008)
14. Luca, A.D., Oriolo, G.: Chapter 7 modeling and control of nonholonomic mechanical systems (2001)
15. Meidenbauer, K.: An investigation of the clothoid steering model for autonomous vehicles. Blacksburg, VA (2007)

16. Murray, R.M., Sastry, S.S.: Nonholonomic motion planning: steering using sinusoids. IEEE Transactions on Automatic Control **38**(5), 700–716 (1993). DOI 10.1109/9.277235
17. Olfati-Saber, R.: Near-identity diffeomorphisms and exponential ϵ -tracking and ϵ -stabilization of first-order nonholonomic $se(2)$ vehicles. Tech. rep. (2002). DOI 10.1109/ACC.2002.1025398
18. Park, M., Lee, S., Han, W.: Development of lateral control system for autonomous vehicle based on adaptive pure pursuit algorithm. In: 2014 14th International Conference on Control, Automation and Systems (ICCAS 2014), pp. 1443–1447 (2014). DOI 10.1109/ICCAS.2014.6987787
19. Siegwart, R., Nourbakhsh, I., Scaramuzza, D.: Introduction to Autonomous Mobile Robots. Intelligent Robotics and Autonomous Agents series. MIT Press (2011). URL <https://books.google.com/books?id=4of6AQAQBAJ>
20. Snider, J.M.: Automatic Steering Methods for Autonomous Automobile Path Tracking. Ph.D. thesis, Carnegie Mellon University (2009)
21. Soltesz, K.: Trajectory tracking control of an autonomous ground vehicle. Ph.D. thesis (2008). DOI 10.13140/RG.2.2.34957.03041
22. Villagra, J., Milanés, V., Pérez, J., Godoy, J.: Smooth path and speed planning for an automated public transport vehicle. Robotics and Autonomous Systems (2012). DOI 10.1016/j.robot.2011.11.001

A Calculating System States for a Unicycle Robot Following a Reference Trajectory

Given a reference trajectory at a specific point in time, $\mathbf{x}_r(t)$, this appendix derives the corresponding unicycle state that would perfectly follow the reference.

The velocity can be found using the first two lines in (1). Note that $[\cos(\psi) \sin(\psi)]^T$ is a unit vector. Assuming $v \geq 0$, v is simply the magnitude of the position derivatives:

$$v = \left\| \begin{bmatrix} \dot{x} \\ \dot{y} \end{bmatrix} \right\| = \sqrt{\dot{x}^2 + \dot{y}^2} \quad (31)$$

The longitudinal acceleration can be found by directly differentiating (31) to obtain

$$a = \dot{v} = \frac{d}{dt} \left(\dot{x}^2 + \dot{y}^2 \right)^{1/2} = (\dot{x}\ddot{x} + \dot{y}\ddot{y}) v^{-1} \quad (32)$$

As the heading is the direction of motion, it can be found using the arc-tangent of the velocity vector:

$$\psi = \text{atan2}(\dot{y}, \dot{x}). \quad (33)$$

Differentiating (33), the angular velocity and acceleration can be found as

$$\omega = \frac{d}{dt} \left(\tan^{-1} \left(\frac{\dot{y}}{\dot{x}} \right) \right) = (\dot{x}\ddot{y} - \dot{y}\ddot{x}) v^{-2} \quad (34)$$

$$\begin{aligned} \alpha &= \frac{d}{dt} (\dot{x}\ddot{y} - \dot{y}\ddot{x}) v^{-2} + (\dot{x}\ddot{y} - \dot{y}\ddot{x}) \frac{d}{dt} (v^{-2}) \\ &= (\dot{x}y^{(3)} - \dot{y}x^{(3)}) v^{-2} - 2(\dot{x}\ddot{y} - \dot{y}\ddot{x}) v^{-3} \dot{v} \\ &= (\dot{x}y^{(3)} - \dot{y}x^{(3)}) v^{-2} - 2a\omega v^{-1} \end{aligned} \quad (35)$$

which gives the results presented in (15).

B Negative Definite Lyapunov Candidate

This appendix shows that (25) holds when $|\psi_{\epsilon r} - \psi| < \frac{\pi}{2}$. Let $e_\psi = \psi_{\epsilon r} - \psi$ and $e_{\psi_r} = \psi_{\epsilon r} - \psi_r$, and let

$$e = \psi - \psi_r = e_{\psi_r} - e_\psi, \quad (36)$$

which allows (25) to be written as

$$\text{sign}(e) = \text{sign}(\sin(e_{\psi_r}) - \sin(e_\psi)). \quad (37)$$

Note that sine is monotonically increasing on the interval $[-\frac{\pi}{2}, \frac{\pi}{2}]$. Thus, to show that (37) holds when $|e_\psi| < \frac{\pi}{2}$, it is sufficient to show that $|e_{\psi_r}| < \frac{\pi}{2}$.

The angle $\psi_{\epsilon r}$ is defined as $\psi_{\epsilon r} = \text{atan2}(\dot{y}_{\epsilon r}, \dot{x}_{\epsilon r})$ where

$$\begin{aligned} \dot{\mathbf{q}}_{\epsilon r} = R_{\epsilon r} \mathbf{y}_r &= \begin{bmatrix} \cos \psi_r & -\epsilon \sin \psi_r \\ \sin \psi_r & \epsilon \cos \psi_r \end{bmatrix} \begin{bmatrix} v_r \\ \omega_r \end{bmatrix} \\ &= \begin{bmatrix} \cos \psi_r \\ \sin \psi_r \end{bmatrix} v_r + \begin{bmatrix} -\sin \psi_r \\ \cos \psi_r \end{bmatrix} \epsilon \omega_r \end{aligned} \quad (38)$$

Since v is constrained to be positive, the direction vector that produces $\psi_{\epsilon r}$ has a component pointing in the same direction as ψ_r . The $\epsilon \omega_r$ term points in a direction orthogonal to that of ψ_r . However, the linear combination of the two vectors will produce a vector oriented in the half-plane defined by ψ_r , thus $|\psi_{\epsilon r} - \psi_r| < \frac{\pi}{2}$ with $|\psi_{\epsilon r} - \psi_r| \rightarrow \frac{\pi}{2}$ as $v \rightarrow 0$ or $\omega \rightarrow \infty$ and $|e_{\psi_r}| < \frac{\pi}{2}$ holds true.